Synthesis and Characterization of Y_2O_3/SiO_2 Composites

C. Cannas, M. Casu, M. Mainas, A. Musinu, and G. Piccaluga

Dipartimento Scienze Chimiche, Cittadella Universitaria,
S.S 554 Km 4.5, 09042, Monserrato (CA), Italy

Reprint requests to A. M.; E-mail: musinu@vaxca1.unica.it

Z. Naturforsch. **59a,** 281 – 287 (2004); received June 3, 2003

Impregnation and deposition-precipitation syntheses have been used to obtain Y_2O_3/SiO_2 samples. In the deposition method, the urea causes the precipitation of yttrium hydroxide, which leads to the formation of yttria nanocrystalline particles in the final composites. Delaying the silica addition up to the visible muddying of the solution, a relevant formation of yttria nanocrystalline particles with average size of about 12 nm is produced. The composites obtained through the impregnation method are amorphous and contain different amounts of yttrium depending on the kind of solvent, the highest concentration being reached using ethanol. In all the samples important interactions at the molecular level among yttrium and silica are revealed, but less important in composites obtained with the deposition precipitation method.

Key words: Deposition; Infiltration; Nanocomposite.

1. Introduction

In the last few decades, yttria (Y_2O_3) has been widely used in a variety of applications including optics, optoelectronics, microelectronics and display devices [1]. Yttria is a superrefractory oxide that finds use as a sintering agent for densifying ceramics [2] such as silicon carbide and nitride or to stabilize the cubic structure of zirconia for applications such as solid electrolyte and oxygen gas sensor. Another interest arises from the use of yttria as insulating host matrix for lanthanide ions in several applications, such as phosphors for fluorescent lighting and cathode ray tubes [3 – 6].

Achieving yttrium oxide crystals in nanosize form results in improved performances compared to coarse grained yttrium oxide. Since free standing nanoparticles are unsuitable for technical applications, it is necessary to employ an optically inert and transparent medium as a host. Amorphous silica is the ideal support both because of its transparency and for the stabilising effect of nanoparticles aggregation. Some authors reported the use of silica for coating [7] or as a dispersing medium on impregnation [8], for doped-yttria nanoparticles. We recently used a sol-gel method in order to obtain yttria nanoparticles dispersed in a silica matrix [9 – 10]. This technique allowed to obtain 2 nm amorphous yttria nanoparticles strongly interacting at the interface with silica.

With the aim of achieving composites with different features as far as the structure and morphology is concerned, two different "two steps" methods were explored; preformed mesoporous commercial silica is adopted as a support, while yttria is dispersed either by a simple impregnation method or by the use of a base as a precipitating agent, both followed by the appropriate thermal treatments. The synthesis by hydrolysis precipitation technique was successfully proposed for preparing doped-Y_2O_3 free standing powders [11]. It seems interesting to apply a similar procedure in order to obtain yttria nanoparticles deposited on the appropriate silica support. An additional goal of the use of the two preparation procedures is to achieve indications about the conditions which affect the formation and the size of nanoparticles. To this end the influence of several process parameters on the final products, like the solvent, impregnation time and temperature, were investigated.

The structural properties of the amorphous and crystalline phases in the final materials and the degree of homogeneity of the particle dispersion as well as their sizes were characterized through TEM and XRD, while the study of the silica support and of the interactions present at the yttria/silica interface was carried out through FTIR and ^{29}Si MAS-NMR spectroscopy.

2. Experimental

The reactants employed were commercial silica (Aldrich, surface area = 300 m^2/g, average pore size = 150 Å), yttrium nitrate ($Y(NO_3)_3{}^*6H_2O$, Aldrich, 99%), absolute ethanol (Carlo Erba) and urea (Aldrich, 99%). Employing fresh silica is a basic requirement in order to obtain the maximum efficiency of impregnation. In fact, physisorption N_2 measurements evidenced a sensible decrease of the specific surface area of aged silica accompanied by a decrease of the average pore diameter. Besides, a degassing procedure of aged silica, performed at 400 °C under high vacuum, needs to be carried out before each preparation in order to obtain reproducible results.

2.1. Impregnation of SiO_2 with Yttrium Nitrate Solutions

1 g of fresh silica was impregnated with 50 ml of aqueous or ethanolic solutions of yttrium nitrate (1.8 Mol). Yttrium nitrate is little soluble in ethanol, therefore a sort of suspension forms instead of a clear solution. The impregnation was performed in three different steps adding two aliquots of 15 ml and one of 20 ml of the original solution to silica and stirring for a total period of 24 hours. The steps of the impregnations were separated by cycles of centrifugation (10 min at 3500 rpm) to remove the liquid before the successive impregnation step. Finally followed by a washing and centrifugation cycle, and then was solid dried at 60 °C for 48 hours. Three samples were prepared following different preparations, systematically varying some process parameters which are reported in Table 1, where the samples are indicated with the labels I1, I2, and I3. A reference sample (I_{ref}) was prepared with the same procedure, but impregnating silica for 24 hours with 50 ml of H_2O. All the samples were submitted to thermal treatments at 900 °C for 1 hr.

2.2. Precipitation onto Silica by Basification of Yttrium Nitrate Solution with Urea

1 g of fresh silica was put in contact with 50 ml of an aqueous solution containing yttrium nitrate (0.29 M), urea (2.4 M) and nitric acid. Two samples, DP1 and DP2, were prepared. In DP1 the silica and the aqueous solution were simultaneously mixed and the suspension stirred for three hours at 80 °C. In DP2 the silica was added to the solution after incipient muddying, caused by the progressive hydrolysis of urea and then stirred for 90 minutes at the same temperature. The use of nitric acid prevents a sharp increase of the pH, avoiding massive precipitation of yttrium hydroxide. The solids were removed from the liquid by centrifugation and then dried at room temperature for 20 hours. Two reference samples were also prepared, that is silica free (DP_{sf}) and yttria free (DP_{ref}), following the same preparation conditions but without the addition of silica in the first case and impregnating silica for three hours with 50 ml of aqueous urea solution in the second one. All the samples were submitted to thermal treatments at 900 °C for 1 hr.

Table 1. Preparation conditions and compositions of all the samples.

Sample	Solvent	Temperature of impregnation	Final pH	Y_2O_3 loading (wt%) (±2%)
I1	Water	Room temperature	2.7	6.9
I2	Water	60 °C	3.6	18.4
I3	Ethanol	Room temperature	0.3	29.2
DP1	Water	80 °C	6.3	13.6
DP2	Water	80 °C	5.4	12.6

The Y_2O_3 loading in all the samples calcined at 900 °C was determined, employing a plasma ICP Perkin Elmer 2000. The results are reported in Table 1.

2.3. Characterization

XRD spectra were collected employing a Seifert diffractometer ID 3000 at Cu Kα wavelength. TEM bright and dark field images were observed with a JEOL 200 CX operating at 200 KV. Mid-IR spectra, from 1500 to 400 cm^{-1}, were obtained using a Bruker EQUINOX 55 spectrophotometer on KBr pellets of the samples.

^{29}Si NMR MAS spectra were collected by using a Varian UNITY INOVA Spectrometer with a 9.39T wide-bore Oxford magnet. The experiments were performed with a probe with 7 mm ZrO_2 rotors at a spinning rate of 6 kHz, and run with a recycle time of 500 s, 45° pulse lengths (4.5 ms), a 100 kHz bandwidth and 200 scans in each experiment. The Q_n distributions in MAS experiments (Q_n represents the SiO_4 tetrahedra sharing *n* bridging oxygens) were obtained by a non-linear fitting of the NMR spectra to individual Gaussians by means of the Origin 4.1 program from Microcal Software. The position, linewidth and intensity were varied in the fitting procedure in order to find the best curve fit to the experimental spectra.

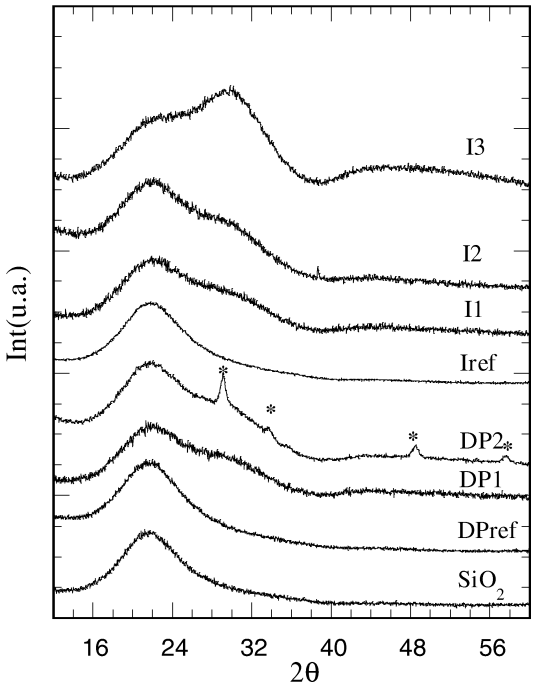

Fig. 1. XRD spectra of all the composites and silica reference samples treated at 900 °C. * Y_2O_3 cubic phase.

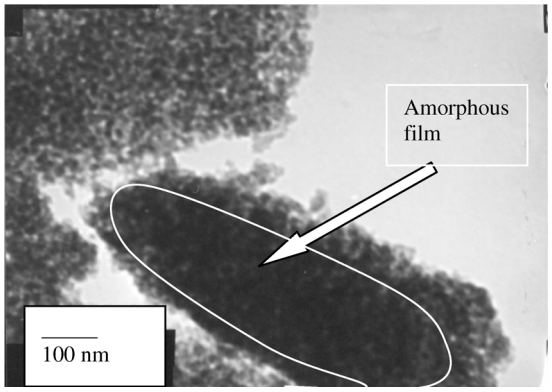

Fig. 2. TEM bright field micrograph of I1 composite treated at 900 °C.

3. Results

3.1. XRD and TEM

The XRD patterns of the I and DP series of samples are reported in Fig. 1 together with that of the silica references, respectively I_{ref} and DP_{ref}, all calcined at 900 °C. The patterns of the silica references are very similar to that of fresh silica calcined at the same temperature. The spectra of samples I1, I2 and I3 show a typical amorphous character and exhibit two main large bands at about $2\theta = 21.3^\circ$ and $2\theta = 29.3^\circ$. The first band is very similar to that of the silica matrix, while the second one grows with yttrium content (Table 1), and therefore can be ascribed to the formation of an yttrium-based disordered phase. Similar features are shown by the spectrum of the sample DP1 obtained by the deposition precipitation method. The spectrum of sample DP2 exhibits a series of crystalline peaks, easily ascribed to the cubic Y_2O_3 phase [12]. The crystalline peaks are quite large, indicating that a nanophase is formed in agreement with TEM results reported below. Moreover, they are superimposed to the pattern of the amorphous silica, but also to the broad band at $2\theta = 29.3^\circ$ already observed in the other samples, which indicates that a fraction of an yttrium-based amorphous phase forms also in this sample.

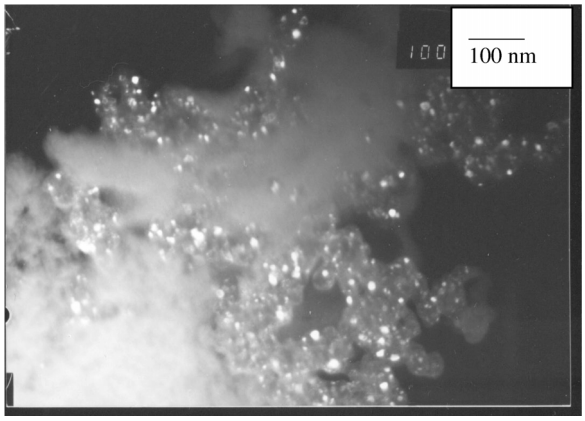

Fig. 3. TEM dark field micrograph of DP2 composite treated at 900 °C.

The amorphous character of the I series of samples is confirmed by the TEM observations. In fact, bright field micrographs show an irregular covering of the porous structure of silica, which is hardly visible in the dark field mode. As an example, a bright field micrograph of sample I1 is shown in Fig. 2, where two portions of the sample can be observed. In the upper part it is evidently the mesoporous structure of naked silica, while in the bottom-right portion the silica texture appears obscured by a sort of amorphous film deposited onto the surface.

On the contrary, Y_2O_3 nanocrystalline particles of spherical shape are evident in sample DP2, both in the bright and in dark field micrographs, as shown in Fig. 3, where a dark field image of this sample is reported. The particle size distribution, calculated for about 650 particles, is reported in Figure 4a. The sizes

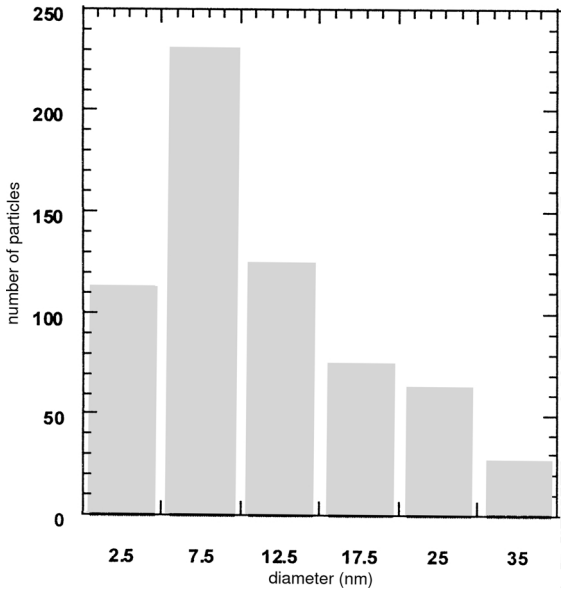

Fig. 4a. Particle size distribution of the DP2 composite.

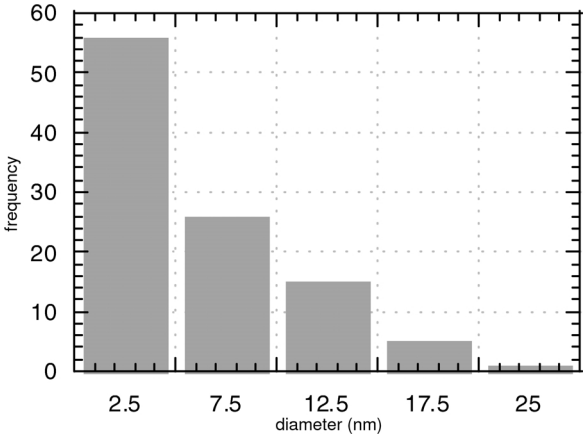

Fig. 4b. Particle size distribution of the DP1 composite.

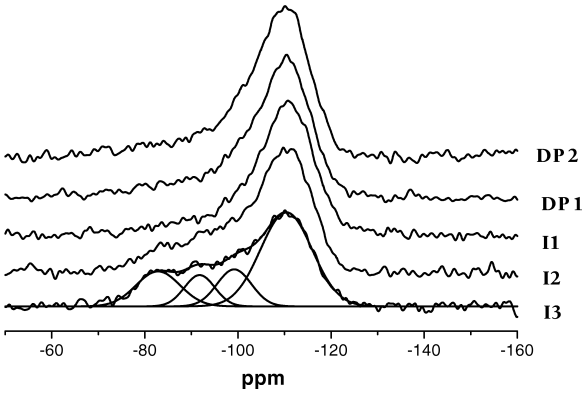

Fig. 5. ^{29}Si MAS-NMR spectra of all composites.

range from 2.5 to 35 nm, with a maximum at 7.5 nm and a mean value of about 12 nm. The sample DP1 exhibits both features already observed in the I series and in sample DP2. In fact, in spite of the amorphous character of the XRD spectrum of sample DP1 and the TEM observation of portions of silica covered by an amorphous film like in the I series, some nanocrystalline particles are visible in dark field mode, though their size (size distribution is reported in Fig. 4b) and amount are much smaller than in sample DP2.

3.2. ^{29}*Si MAS-NMR*

The ^{29}Si-MAS NMR spectra of all the composite samples, shown in Fig. 5, exhibit a main peak at about 110 ppm ascribed to Q_4 groups, standing beside very intense low field components in sample I3. The spectrum of sample I3 was interpreted in terms of four overlapping signals falling in the -70 to -120 ppm range. A good simulation using four gaussians allowed the following assignments: Q_4 (-110 ppm), Q_3 (-100 ppm), Q_2 (-93 ppm) and Q_1 (-84 ppm) groups, according to [10, 13]. The result from the best fit is reported in Table 2. The Q_3 and Q_2 groups have fwhm values (Q_3, 9.0 ppm, and Q_2, 6.8 ppm) quite similar to that of the silica sample (9.4 ppm and 7.0 ppm respectively) [10], suggesting that they are far from the yttrium centres and so are unaffected by the presence of metal ions. The presence of the large Q_1 signal (fwhm 11.2 ppm), absent in the I_{ref} sample, can be explained by a larger chemical and structural diversity of environments, and therefore the Si-O-H groups can be partly or totally substituted by Si-O-Y bonds. This attribution to Q_1 groups is also justified by its chemical shift value, which is consistent with that of the Q_1 found in similar composites treated at higher temperatures and typical of h-$Y_2Si_2O_7$ silicate reported in [10, 13]. This is an indication that an interaction is present between the nanoparticles and the matrix at the molecular level. The percentage of Q_1 sites in sample I3 accounts for the bonding of the whole amount of yttrium ions to the silica matrix, since its value (21%) is comparable to the amount of yttrium (23 at %) present in this composite.

The spectra of samples I1 and I2 show a similar profile, but the low field signals are less pronounced. An estimate of the integrated area of these signals was obtained by using the chemical shift of the Q_3, Q_2, and

Table 2. Q_n sites percentage (accuracy 3 – 6%) resulted from the simulation of ^{29}Si MAS NMR spectra of all the samples.

Sample	Q_4	Q_3	Q_2	Q_1	Y (at %)
I1	79	13	4	4	5.4
I2	65	16	8	11	14.5
I3	57	15	7	21	23
DP1	73	16	6	5	10.7
DP2	72	17	6	5	9.9

Q_1 bands found in the I3 sample as constraints for the deconvolution; the results from the best fit are reported in Table 1. The results found for samples I1 and I2, in terms of the relationship between the amount of yttrium and the percentage of Q_1 groups, show a behaviour very similar to sample I3, suggesting that yttrium is totally interacting at a molecular level with the surface of the silica matrix. This can be interpreted with the formation of an amorphous yttrium-based silicate phase covering the silica surface, in agreement with the TEM bright field observation (Fig. 2) and the XRD results (Fig. 1).

The spectra of the samples DP1 and DP2 exhibit similar features. The integrated area of these signals was estimated with the same procedure as used for the I1 and I2 spectra; the results from the best fit are reported in Table 2. Differently from the I series, in DP samples the Q_1 percent (5%) is roughly one half of the percentage of the yttrium atoms (10%). Therefore, this signal does not account for a complete chemical interaction of yttrium ions with the silica matrix. In such a case, greater values of the Q_1 sites should have been observed.

3.3. IR

Figure 6 shows the IR spectra between 1500 and 400 cm^{-1} of all the composite samples. In all the samples the typical antisymmetric stretching modes at 1238, 1112 cm^{-1} and the symmetric stretching modes at 795 cm^{-1} of Si-O-Si bridges as well as that of the O-Si-O bending at 473 cm^{-1} are present [14 – 16]. All the spectra are characterised by a broad shoulder in the region between 980 and 870 cm^{-1}, partially overlapping the band at 800 cm^{-1}; this shoulder is most evident in the sample I3, and only slightly evident in samples I1, DP1 and DP2. This band can be ascribed to the Si-O-H stretching, consistently with previously investigated samples treated at 900 °C [10], but also to the Si-O-Y stretching already assigned in the spectrum of yttrium silicate [17]. Since the intensity of this shoulder increases with yttrium oxide concentration in the I series,

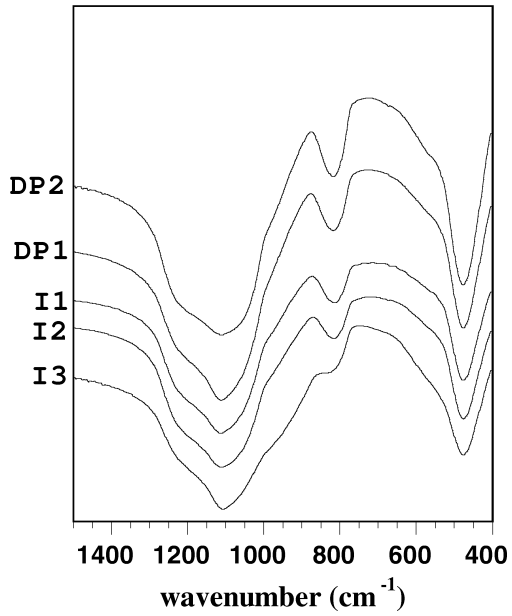

Fig. 6. FTIR spectra of all composites.

this band can be mainly ascribed to Si-O-Y stretching, while its broadening can be related to a variety of different bond lengths and angles in a structurally disordered silicate, according to NMR results. The intensity of the band in the spectra of samples DP1 and DP2 is very similar to that of sample I1 in spite of the different yttrium content. This finding, correlated with NMR results, indicates that the number of Si-O-Y bonds in the DP series is much lower than that of the I series.

4. Discussion

The composites obtained by simple impregnation (I series) and deposition-precipitation (DP series) exhibit different features both from the points of view of structure and yttrium-silica interactions, going from samples I where an amorphous yttrium silicate is spread over the silica surface, to sample DP2 where crystalline yttria nanoparticles are stabilised onto the silica matrix.

The different behaviour can be partially interpreted considering the evolution along thermal treatments of different precursors deposited onto the matrix at the preliminary stages of preparation. In fact, the yttrium nitrate pentahydrate phase was identified in the XRD pattern of an I3 dried sample (not reported). This is the precursor which evolves towards the formation of amorphous yttrium silicate at 900 °C in the I series (Fig. 1). Conversely, yttrium hydroxide, formed at the

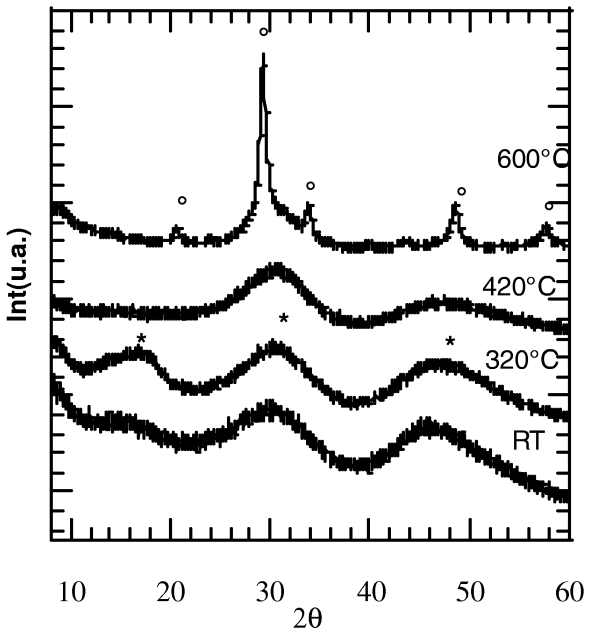

Fig. 7. XRD spectra of the free silica sample (ppt) as a function of thermal treatments. * $Y(OH)_3$ and ° Y_2O_3 cubic phase.

higher pH values determined by urea hydrolysis (Table 1), is the precursor of the yttria particles in the DP series. In fact, though in the amorphous XRD patterns of the dried samples of the DP series this phase is hardly visible, its presence was clearly demonstrated by the investigation of the free silica sample (DP_{sf}). In Fig. 7, the XRD patterns of DP_{sf} as a function of thermal treatments are reported. The spectra of samples treated at temperatures lower than 700 °C exhibit the evolution of three large bands, whose position is ascribable to the main peaks of $Y(OH)_3$ [18]. This phase transforms completely at 700 °C into the cubic Y_2O_3 phase, already found in the DP2 sample (Fig. 1). This result is also in good agreement with that reported in the literature for free-standing doped-yttrium oxide nanoparticles [11] obtained by a precipitation method.

Minor but significant differences are also present inside each series. The enhancement of the broad band at $2\theta = 29.3^\circ$ in the XRD spectra along the samples I1, I2, I3 can be easily correlated with the increasing yttrium concentration, consistent with the values reported in Table 1. This result indicates that the use of ethanol as impregnation solvent is more efficient for achieving high concentrations of yttrium in the final composite. The whole behaviour can be ascribed to the peculiar conditions used in the impregnation step. In fact, the use of ethanol instead of water and/or the higher impregnation temperature causes a lowering of the viscosity of the solution, which easily enters the cavities covering more effectively the irregular silica surface. As a consequence of the successive thermal treatments, a reaction with the silica surface takes place with the formation of an amorphous yttrium silicate covering the surface, as revealed by TEM, IR and NMR spectroscopy.

As far as the DP series is concerned, a similar extent of yttrium/silica interactions was found in both samples. However, only the method which delays the silica addition up to the visible muddying of the solution produces the formation of yttria nanocrystalline particles with the required sizes. In fact, yttria nanocrystalline particles with average sizes of about 12 nm are well recognizable by XRD and TEM in the DP2 sample. This result is unambiguously connected with the precursor phase formed at the early stage of impregnation, but mostly with its particle size. If the precursor is yttrium hydroxide, but it precipitates over the silica before the particles reach a critical size, it is likely that the prompt establishing of a cohesion with the matrix surface hampers their coalescence and growth during the thermal treatment. This seems the case for the DP1 sample, where the final composite is constituted partially by a low amount of (5 nm) yttria nanoparticles. Moreover, at the early stages of preparation of sample DP1, before the pH has reached the value adequate for the yttrium hydroxide precipitation, the silica can be impregnated in a similar way as in the I series. This may account for the amorphous yttrium-based phase spread over silica, observed in sample DP1.

The particle size distribution of the DP samples (mostly DP2) is spread over a range which is useful for the achievement of luminescent materials, after the appropriate synthesis of a silica based composite containing Eu^{3+}doped-yttria nanoparticles. Recently, luminescence measurements of a Eu^{3+} doped-yttria/silica nanocomposite treated at 1000° were performed, which indicate that the sites in which the Eu^{3+} ions are accommodated are disordered and that the decay times of the $^5D_0$ emission are rather long, suggesting that multiphonon relaxation is not effective in quenching the luminescence [19].

5. Conclusion

Impregnation and deposition precipitation syntheses have been used for the achievement of Y_2O_3/SiO_2 composites.

In the deposition method, the addition of urea causes the precipitation of yttrium hydroxide which is the precursor of yttria nanocrystalline particles in the Y_2O_3/SiO_2 nanocomposites. However, the most promising synthesis was the one where the addition of silica is delayed up to the visible muddying of the solution. In this case a relevant formation of yttria nanocrystalline particles with the sizes of about 12 nm is produced in the final samples.

Through the impregnation method amorphous samples were obtained, containing different amounts of yttrium as functions of the kind of solvent, the highest concentration being reached using ethanol. In all the samples important interactions at the molecular level among yttrium and silica were revealed, with a lesser amount in the samples obtained with the deposition method.

Acknowledgements

This work was carried out within the MURST PRIN project 9903222581_005.

[1] A. M. Lejeus and R. Collongues, Current Topics in Material Science. In: Kaldis E. editor, North–Holland Publ. Company, Amsterdam, **Vol. 4**, p. 481 (1980).
[2] T. B. Troczynski and P. S. Nicholson, J. Amer. Ceram. Soc. **72**, 1488 (1989).
[3] G. Blasse and B. C. Grabmaier, Luminescent Materials, Springer-Verlag, Berlin 1994.
[4] T. Ye, Z. Guiwen, Z. Weiping, and X. Shangda, Mater. Res. Bull. **3**, 501 (1997).
[5] B. M. Tissue, Chem. Mater. **10**, 2837 (1998).
[6] E. T. Golburt, B. Kulkarni, R. N. Bhargava, J. Taylor, and M. Libera, J. Lumin, **72**, 190 (1997).
[7] Q. Li, L. Gao, and D. Yan, Chem. Mater. **11**, 533 (1999).
[8] R. Schmechel, M. Kenedy, H. Von Seggem, H. Winkler, M. Kolbe, R. A. Fischer, Li Xaomao, A. Benker, and M. H. Winterer, J Appl.Phys. **89**, 1679 (2001).
[9] C. Cannas, M. Casu, A. Musinu, G. Piccaluga, A. Speghini, and M. Bettinelli, J. Non Cryst. Solids **193**, 306 (2002).
[10] C. Cannas, M. Casu, A. Lai, A. Musinu, and G. Piccaluga, Phys. Chem., Chem. Phys. **4**, 2286 (2002).
[11] Y. D. Jiang, Z. L. Wang, F. Zhang, H. G. Paris, and C. J. Summers, J. Mater. Res. **13**, 2950 (1999).
[12] Powder Diffraction File Card N° 43-1036 International Center for Diffraction Data, 1998, Swarthmore, PA USA.
[13] E. Lippmaa, M. Magi, A. Samoson, G. Enghelhardt, and A. R. Grimmer, J. Amer. Chem. Soc. **102**, 4889 (1980).
[14] A. Bertoluzza, C. Fagnano, M. A. Morelli, V. Gottardi, and M. Guglielmi, J. Non-Cryst. Solids **48**, 117 (1982).
[15] P. Hofmann and E. Knozinger, Surf. Sci. **188**, 181 (1987).
[16] D. L. Wood and E. M. Rabinovich, Appl. Spectrosc. **43**, 263 (1989).
[17] J. J. Chambers and G. N. Parsons, J. Appl. Phys. **90**, 918 (2001).
[18] Powder Diffraction File Card N° 24-1422 International Center for Diffraction Data, 1998, Swarthmore, PA USA.
[19] C. Cannas, M. Casu, M. Mainas, A. Musinu, G. Piccaluga, S. Polizzi, A. Speghini, and M. Bettinelli, J. Mater. Chem. **13**, 1 (2003).